Hybrid Polymer Particles with a Protective Shell: Synthesis, Structure, and Templating

Lyudmila M. Bronstein,*[,†] Suraj Dixit,[†] John Tomaszewski,[†] Barry Stein,[‡] Dmitri I. Svergun,[§,||] Peter V. Konarev,[§,||] Eleonora Shtykova,[§] Ulrike Werner-Zwanziger,[⊥] and Bogdan Dragnea[†]

Departments of Chemistry and Biology, Indiana University, Bloomington, Indiana 47405, Institute of Crystallography, Russian Academy of Sciences, 59 Leninsky pr., 117333 Moscow, Russia, European Molecular Biology Laboratory, Outstation, Notkestrasse 85, D-22603 Hamburg, Germany, Department of Chemistry, Dalhousie University, Halifax, NS, B3H 4J3 Canada

Received January 18, 2006. Revised Manuscript Received March 3, 2006

The development of hybrid polymer particles formed by the hydrolytic condensation of octadecyldimethyl(3-trimethoxysilylpropyl)ammonium chloride (ODMACl) and the trisodium salt of the triacetic acid N-(trimethoxysilylpropyl)ethylenediamine (TANED) along with self-assembling with nonionic poly(ethylene glycol) (PEG) based surfactants containing a hydrophobic octadecyl tail (Brij) have been studied using liquid and solid-state NMR, dynamic light scattering (DLS), transmission electron microscopy, differential scanning calorimetry (DSC), X-ray diffraction (XRD), and small-angle X-ray scattering (SAXS). On the basis of DLS and NMR data, the mechanism of interaction of Brij, ODMACl, and TANED molecules in an aqueous solution has been suggested. The influence of the PEG chain length on the ability of surfactants to stabilize polymer particles has been established. The combination of DSC and XRD assessed the crystallinity and thermal properties of self-assembled hybrid materials in the solid state, while SAXS studies revealed that their morphology strikingly depends on the PEG chain length and reaction conditions determining the degree of Brij incorporation and the structure of the Brij−ODMACl complex. Because of the protective PEG shell, the hybrid polymer particles were successfully used as soluble templates for the formation of iron oxide nanoparticles.

Introduction

Polymer particles such as block copolymer micelles, latex particles, microgels, and other hybrid particles received considerable attention because of their prospective applications as drug delivery agents,[1−6] templates for nanoparticle formation,[7−15] or advanced organic and inorganic materials.[16−22] In our earlier work,[23] we reported the synthesis of polymer particles by the simple hydrolytic condensation of a mixture of two silanes (see Chart 1): one bearing the quaternary ammonium group [octadecyldimethyl(3-trimethoxysilylpropyl)ammonium chloride, ODMACl] and the other bearing the carboxylate group [the trisodium salt of the triacetic acid N-(trimethoxysilylpropyl)ethylenediamine, TANED].

These two silanes form gegenions, and their simultaneous hydrolytic condensation results in polymer particles containing two types of functional groups. The ability of these particles to serve as templates for controlled nanoparticle formation and positioning was reported earlier.[23] However, the incorporation of metal compounds and metal nanoparticle formation result in strong interactions between polymer

* To whom correspondence should be addressed. Phone: 1-812-855-3727. Fax: 1-812-855-8300. E-mail: lybronst@indiana.edu.
† Department of Chemistry, Indiana University.
‡ Department of Biology, Indiana University.
§ Russian Academy of Sciences.
|| EMBL, Outstation.
⊥ Dalhousie University.

(1) Cohen, H.; Levy, R. J.; Gao, J.; Fishbein, I.; Kousaev, V.; Sosnowski, S.; Slomkowski, S.; Golomb, G. *Gene Ther.* **2000**, *7*, 1896.
(2) Pignatello, R.; Bucolo, C.; Puglisi, G. J. *Pharm. Sci.* **2002**, *91*, 2636.
(3) Ahlin, P.; Kristl, J.; Kristl, A.; Vrecer, F. *Int. J. Pharm.* **2002**, *239*, 113.
(4) Kim, I.-S.; Kim, S.-H. *Int. J. Pharm.* **2003**, *257*, 195.
(5) Pan, D.; Turner, J. L.; Wooley, K. L. *Macromolecules* **2004**, *37*, 7109.
(6) Qi, K.; Ma, Q.; Remsen, E. E.; Clark, C. G., Jr.; Wooley, K. L. *J. Am. Chem. Soc.* **2004**, *126*, 6599.
(7) Spatz, J. P.; Roescher, A.; Möller, M. *Adv. Mater.* **1996**, *8*, 337.
(8) Bronstein, L. M.; Linton, C.; Karlinsey, R.; Stein, B.; Svergun, D. I.; Zwanziger, J. W.; Spontak, R. J. *Nano Lett.* **2002**, *2*, 873.
(9) Antonietti, M.; Wenz, E.; Bronstein, L.; Seregina, M. *Adv. Mater.* **1995**, *7*, 1000.
(10) Moffitt, M.; McMahon, L.; Pessel, V.; Eisenberg, A. *Chem. Mater.* **1995**, *7*, 1185.
(11) Underhill, R. S.; Liu, G. *Chem. Mater.* **2000**, *12*, 2082.
(12) Zhao, M.; Crooks, R. M. *Chem. Mater.* **1999**, *11*, 3379.
(13) Masuhara, H.; Nakanishi, H.; Sasaki, K. *Single Organic Nanoparticles*; Springer-Verlag: Berlin, 2003.
(14) Gorelikov, I.; Field, L. M.; Kumacheva, E. *J. Am. Chem. Soc.* **2004**, *126*, 15938.
(15) Bronstein, L. M.; Linton, C.; Karlinsey, R.; Ashcraft, E.; Stein, B.; Svergun, D. I.; Kozin, M.; Khotina, I. A.; Spontak, R. J.; Werner-Zwanziger, U.; Zwanziger, J. W. *Langmuir* **2003**, *19*, 7071.
(16) Liu, T.; Burger, C.; Chu, B. *Prog. Polym. Sci.* **2003**, *28*, 5.
(17) Mezzenga, R.; Ruokolainen, J.; Fredrickson, G. H.; Moses, D.; Heeger, A. J.; Ikkala, O. *Science* **2003**, *299* (5614), 1872.
(18) Jung, M.; den Ouden, I.; Montoya-Goni, A.; Hubert, D. H. W.; Frederik, P. M.; van Herk, A. M.; German, A. L. *Langmuir* **2000**, *16*, 4185.
(19) Förster, S. *Top. Curr. Chem.* **2003**, *226*, 1−28.
(20) Xu, S.; Zhang, J.; Paquet, C.; Lin, Y.; Kumacheva, E. *Adv. Funct. Mater.* **2003**, *13*, 468.
(21) Pham, H. H.; Kumacheva, E. *Macromol. Symp.* **2003**, *192*, 191.
(22) Alteheld, A.; Gourevich, I.; Field, L. M.; Paquet, C.; Kumacheva, E. *Macromolecules* **2005**, *38*, 3301.
(23) Bronstein, L. M.; Linton, C.; Karlinsey, R.; Stein, B.; Timofeeva, G. I.; Svergun, D. I.; Konarev, P. I.; Kozin, M.; Tomaszewski, J.; Werner-Zwanziger, U.; Zwanziger, J. W. *Langmuir* **2004**, *20*, 1100.

10.1021/cm060129t CCC: $33.50
Published on Web 03/31/2006

Chart 1

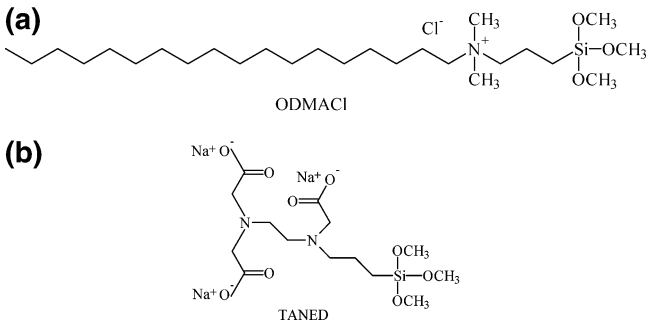

particles, leading to aggregation. To prevent this aggregation, we suggest using nonionic surfactants, the incorporation of which inside poly(ODMACl−TANED) particles will create the protective shell around the particles.

Hybrid structures consisting of polymers and surfactants are well-known. The addition of surfactants was used to form highly ordered complexes with linear[24,25] or cross-linked polyelectrolytes,[26−29] to stabilize globular aggregates of thermoresponsive polymers in aqueous solutions,[30] and to functionalize or modify block copolymer micelles.[31−37] When polyelectrolyte complexes are formed or functionalization is desired, normally, ionic surfactants are employed, while for solubilization or stabilization, nonionic surfactants can be used. On the other hand, several papers describing the interaction of sodium dodecyl sulfate (SDS) and some other surfactants with Pluronics [poly(ethylene oxide)-*block*-poly(propylene oxide)-*block*-poly(ethylene oxide), PEO_x-PPO_y-PEO_x] reported decomposition of the block copolymer micelles upon complexation with surfactant molecules,[38−40] which progressed with an increase of the SDS concentration. This was due to strong binding of a surfactant molecule to a hydrophobic block of Pluronics, completely suppressing Pluronic micellization. In this paper, we report the formation of composite poly(ODMACl−TANED) particles with a protective shell formed by the incorporation of nonionic poly(ethylene glycol) (PEG) based surfactants (Brij). We discuss the mechanism of the hybrid micelle formation and the influence of the PEG chain length on the ability of surfactants to stabilize polymer particles and on self-assembling in a solid state. The hybrid particles' ability to serve as soluble templates for iron oxide nanoparticle formation is also demonstrated.

(24) Antonietti, M.; Conrad, J.; Thuenemann, A. *Macromolecules* **1994**, *27*, 6007.
(25) Antonietti, M.; Henke, S.; Thuenemann, A. *Adv. Mater.* **1996**, 8, 41.
(26) Chu, B.; Yeh, F.; Sokolov, E. L.; Starodoubtsev, S. G.; Khokhlov, A. R. *Macromolecules* **1995**, *28*, 8447.
(27) Yeh, F.; Sokolov, E. L.; Khokhlov, A. R.; Chu, B. *J. Am. Chem. Soc.* **1996**, *118*, 6615.
(28) Hansson, P.; Schneider, S.; Lindman, B. *J. Phys. Chem. B* **2002**, *106*, 9777.
(29) Bronstein, L. M.; Platonova, O. A.; Yakunin, A. N.; Yanovskaya, I. M.; Valetsky, P. M.; Dembo, A. T.; Makhaeva, E. E.; Mironov, A. V.; Khokhlov, A. R. *Langmuir* **1998**, *14*, 252.
(30) Makhaeva, E. E.; Tenhu, H.; Khokhlov, A. R. *Macromolecules* **1998**, *31*, 6112.
(31) Bronstein, L. M.; Chernyshov, D. M.; Timofeeva, G. I.; Dubrovina, L. V.; Valetsky, P. M.; Khokhlov, A. R. *J. Colloid Interface Sci.* **2000**, *230*, 140.
(32) Bronstein, L. M.; Chernyshov, D. M.; Timofeeva, G. I.; Dubrovina, L. V.; Valetsky, P. M.; Obolonkova, E. S.; Khokhlov, A. R. *Langmuir* **2000**, *16*, 3626.
(33) Hu, Z.; Jonas, A. M.; Varshney, S. K.; Gohy, J.-F. *J. Am. Chem. Soc.* **2005**, *127* (18), 6526−6527.
(34) Jansson, J.; Schillen, K.; Nilsson, M.; Soederman, O.; Fritz, G.; Bergmann, A.; Glatter, O. *J. Phys. Chem. B* **2005**, *109*, 7073.
(35) Berret, J.-F.; Vigolo, B.; Eng, R.; Herve, P.; Grillo, I.; Yang, L. *Macromolecules* **2004**, *37*, 4922.
(36) Bronich, T. K.; Popov, A. M.; Eisenberg, A.; Kabanov, V. A.; Kabanov, A. V. *Langmuir* **2000**, *16*, 481.
(37) Kunieda, H.; Kaneko, M.; Lopez-Quintela, M. A.; Tsukahara, M. *Langmuir* **2004**, *20*, 2164.
(38) Hecht, E.; Hoffmann, H. *Langmuir* **1994**, *10*, 86.
(39) Hecht, E.; Mortensen, K.; Gradzielski, M.; Hoffmann, H. *J. Phys. Chem.* **1995**, *99*, 4866.
(40) Zhang, K.; Lindman, B.; Coppola, L. *Langmuir* **1995**, *11*, 538.

Table 1. Material Notations and Experimental Parameters

notation	type of Brij	ODMAC:Brij (mol)	equilibration time
O-B76-T2A	Brij 76	1:6	30 min
O-B76-T2A-2-prec	Brij 76	1:2	30 min
O-B76-T2A-2-sol	Brij 76	1:2	30 min
O-B78-T2A	Brij 78	1:6	30 min
O-B700-T2A	Brij 700	1:6	30 min
O-B78-T2	Brij 78	1:6	2 h
O-B78-T2B	Brij 78	1:6	24 h
O-B78-T2B-Fe_2O_3	Brij 78	1:6	24 h

Experimental

Materials. ODMACl (as a 60% solution in methanol) and TANED (as a 45% solution in water) were purchased from Gelest and used as received. Brij 76, 78, and 700, nonionic surfactants with the PEG block of various length: where $n = 10$ for Brij 76,

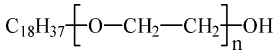

$n = 20$ for Brij 78, and $n = 100$ for Brij 700, were purchased from Aldrich and used as received. $FeCl_3 \cdot 6H_2O$ (98%, LabGuard) and H_2O_2 (50%, Fisher Chemical) were used as received. Water was purified with a "Barnstead NANOpure water" purification system.

Synthesis

Hybrid Polymer Particles Based on ODMACl, TANED, and Brij 76 (Brij 78 or Brij 700). In a typical experiment for molar ratio Brij/ODMACl = 1:6, 0.0332 g (0.047 mmol) of Brij 76 was dissolved in 20 mL of deionized water at 60 °C for 30 min and then stirred for 24 h at room temperature. After that, 0.232 g of a 60% ODMACl solution in methanol (0.280 mmol) was added to the Brij 76 solution and kept stirring for 30 min (2 or 24 h) for equilibration. Then, 0.287 g of a 45% TANED aqueous solution (0.280 mmol) was added dropwise. No pH adjustment was necessary because TANED gives a pH of 10 in the reaction solution. Upon TANED addition, the solution immediately became turbid, and a white precipitate formed within 30 min. After 2 h of stirring, the precipitate was isolated by filtration, washed several times with cold water and a cold water/methanol mixture, and dried overnight in a vacuum oven at 30 °C. For Brij 78 and Brij 700, colloidal solutions were formed. To remove unreacted TANED, a 3-fold purification of these reaction solutions was carried out in an Amicon ultrafiltration cell with a 3000 Da cutoff membrane. After the last purification, the concentrated solution was evaporated at 60 °C and then dried in a vacuum oven at 30 °C. For Brij 76 at a molar ratio Brij/ODMACl = 1:2, the reaction solution contained both a precipitate and a colloidal solution; the two were separated first by filtration, and then the colloidal solution was purified by ultrafiltration.

The notations of all of the samples and experimental parameters are presented in Table 1.

Templating with O-B78-T2 was carried out similarly to the method described elsewhere.[11] In a typical experiment, 10 mL of the O-B78-T2B ultrafiltrated solution was diluted by a factor of 10 with deinozed water, purged with argon for 60 min, and charged with 0.042 g (0.141 mmol) of $(NH_4)_2Fe(SO_4)_2 \cdot 6H_2O$ dissolved in 1 mL of water and purged with argon for 30 more minutes. The reaction mixture was kept stirring at room temperature for 2−3 days. After that, the reaction solution was ultrafiltrated to remove nonreacted salt, the pH was adjusted with an aqueous ammonia solution to 10.0, and the solution was purged with argon. Then, 0.1 mL of H_2O_2 was added, and the reaction mixture was stirred for 24 h. The final solution was again ultrafiltrated three times to remove all side products. After the last ultrafiltration, the concentrated solution was evaporated at 60 °C and dried in a vacuum oven at 30 °C. By elemental analysis, the Fe content is 5.30 wt %. This represents the incorporation of 77.5% of the iron employed.

Characterization

The liquid-state ^{13}C NMR spectra of the hybrid samples well-soluble in $CDCl_3$ were recorded on VarianUNITYINOVA spectrometers operated at either 9.40 or 11.74 T (Larmor frequencies: 100.5 or 125.7 MHz, respectively). Peak assignments were performed using the ACD/CNMR Spectrum Generator 8.0 software. Solid-state ^{13}C (for O-B700-T2) and ^{29}Si NMR spectra were acquired on a Bruker DSX Avance spectrometer using a 9.4 T magnet, magic angle spinning (MAS), and cross polarization (CP) from protons. The ^{13}C CP/MAS NMR spectra were recorded using rotors of 4 mm diameter and spinning up to 11 kHz. The ^{29}Si CP/MAS NMR experiments were performed using rotors of 7 mm diameter. The spinning speeds were varied up to 6.00 kHz to distinguish spinning sidebands from the center band.

FT-IR spectra were recorded on a Nicolet A320 spectrometer in the range 400−4000 cm^{-1} with a 2 cm^{-1} resolution using the AVATAR 360 accessory.

Powder diffraction patterns were collected on a Scintag $\theta-\theta$ powder diffractometer with a Cu Kα source (1.54 Å).

Differential scanning calorimetry (DSC) was performed using a Q10 TA calorimeter operating in low-temperature mode with liquid N_2 as the coolant. Both cyclohexane and indium were used to calibrate transitions. Samples weighing between 5 and 12 mg were sealed in aluminum pans and heated once from −100 °C to +150 °C at a rate of 10 °C/min.

Electron-transparent specimens for transmission electron microscopy (TEM) were prepared by placing a drop of dilute solution onto a carbon-coated Cu grid. TEM samples of nonmetalated polymer particles were stained with OsO_4 vapor for 30 min. Images were acquired at an accelerating voltage of 60 kV on a JEOL JEM1010 transmission electron microscope.

Dynamic light scattering (DLS) measurements were carried out in aqueous solutions with the Malvern Instruments Zetasizer Nano-6. DLS experiments were carried out at a 90° scattering angle and at 25 °C.

The small-angle X-ray scattering (SAXS) data were collected on the X33 camera with a linear gas detector and a MAR345 Image Plate detector[41−43] of the European Molecular Biology Laboratory on the storage ring DORIS III of the Deutsches Elektronen Synchrotron (DESY, Hamburg). The powders were measured in cuvettes with mica windows with a sample thickness of 1 mm at room temperature. The scattering patterns were recorded at the wavelength $\lambda = 0.15$ in the range of momentum transfer $0.1\ nm^{-1} < s < 5.2\ nm^{-1}$ [$s = (4\pi/\lambda) \sin\theta$, where 2θ is the scattering angle].

The quasi-periodic structures formed in the semicrystalline hybrid materials gave rise to Bragg peaks in the isotropic scattering patterns. These peaks were analyzed to characterize the type of ordering following standard procedures using the programs PRIMUS and PEAK.[44]

Lamellar structures were characterized by equidistant sequences of reflections: $s_n = 2\pi n/d_1$, $n = 1, 2, 3$, and so forth, where $d_1 = 2\pi/s_1$ is the periodicity of the ordered motifs computed from the position of the first peak in the scattering pattern. The two-dimensional hexagonal phase of long cylindrical micelles was determined by the sequence of Bragg reflections: $s_n = 2\pi(2/\sqrt{3})\sqrt{n}/d_1$, $n = (h^2 + k^2 + hk)$, where h and k are integer Miller indices, and the lateral separation between the micelles was calculated as $d_{hex} = 2d_1/\sqrt{3}$. For the cubic phases, Bragg reflections occur at positions $s_n = 2\pi\sqrt{n}/d_1$, $n = (h^2 + k^2 + l^2)$, where h, k, and l are integers. The cubic cell periodicity is either $d_c = d_1 = 2\pi/s_1$ (for the first observable reflection with Miller indices $hkl = 100$) or $d_c = d_1\sqrt{2}$ (for the first reflection with $hkl = 110$).

The mean long-range order dimension, L (the size of crystallites), and the degree of disorder in the system, Δ/d_1, were calculated as[45]

$$L = \frac{\lambda}{\beta_s \cos\theta_1} \tag{1}$$

$$\Delta/d_1 = \frac{1}{\pi}\sqrt{\frac{\beta_s d_1}{\lambda}} \tag{2}$$

where β_s is the full width at a half-maximum intensity of a peak (in radians) observed at a mean scattering angle of $2\theta_1$, corresponding to the momentum transfer s_1, and Δ is the mean-square deviation of distances between neighboring regularly packed structure motifs.

Results and Discussion

1. Formation of Hybrid Polymer Particles in Aqueous Solutions. *1.1. Strategy and Synthesis.* Our strategy in developing the protective shell was based on our earlier study of mixed micelles formed by an amphiphilic block copolymer, polystyrene-*block*-poly(ethylene oxide) (PS-*b*-PEO), and anionic and cationic surfactants.[31,32,46] We demonstrated that surfactants are incorporated into the block copolymer micelles (instead of the formation of surfactant micelles) even at the concentrations exceeding the surfactant critical micelle concentration (CMC). Considering that Brij molecules resemble PS-*b*-PEO[31,32] and the cationic surfactant (cetylpyridinium chloride) is similar to ODMACl, we surmised that, if ODMACl is added to the solution of Brij micelles, the hydrophobic tails of ODMACl molecules will enter the Brij micelles forming mixed (or hybrid) micelles. When TANED molecules are added, they will tend to form an electrolyte complex with ODMACl, thus entering the mixed micelles. The formation of these complexes induces im-

(41) Koch, M. H. J.; Bordas, J. *Nucl. Instrum. Methods* **1983**, *208*, 461.
(42) Boulin, C. J.; Kempf, R.; Gabriel, A.; Koch, M. H. J. *Nucl. Instrum. Methods* **1988**, *269*, 312.
(43) Gabriel, A.; Dauvergne, F. *Nucl. Instrum. Methods* **1982**, *201*, 223.
(44) Konarev, P. V.; Volkov, V. V.; Sokolova, A. V.; Koch, M. H. J.; Svergun, D. I. *J. Appl. Crystallogr.* **2003**, *36*, 1277.
(45) Vainshtein, B. K. *Diffraction of X-rays by Chain Molecules*; Elsevier Publishing Company: Amsterdam, 1966.
(46) Bronstein, L. M.; Chernyshov, D. M.; Vorontsov, E.; Timofeeva, G. I.; Dubrovina, L. V.; Valetsky, P. M.; Kazakov, S.; Khokhlov, A. R. *J. Phys. Chem. B* **2001**, *105*, 9077.

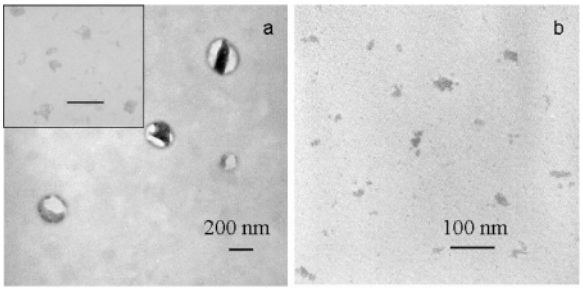

Figure 1. TEM images of O-B76-T2A (a), O-B76-T2A-2 (inset in a), and O-B78-T2A (b). The scale bar in the inset is 200 nm.

mediate hydrolytic condensation of the ODMACl−TANED complex as discussed in our preceding paper.[23]

In this work, we studied the development of a protective hydrophilic shell with nonionic surfactants containing an octadecyl hydrophobic tail, $C_{18}H_{37}$, and hydrophilic PEG tails with 10 (Brij 76), 20 (Brij 78), and 100 (Brij 700) repeated units. To minimize the likelihood of the existence of empty Brij micelles in the reaction solution, we chose a molar ratio of Brij to ODMACl of 1:6.

When Brij 76 is used in the hybrid micelle formation, the precipitate is formed soon after the addition of TANED, similar to pristine poly(ODMACl−TANED) described earlier.[23] The final product, O-B76-T2 (see notations in the Experimental section), dissolves in methanol, forming a colloidal solution. A TEM image of this sample stained with OsO_4 is shown in Figure 1a. One can see large complex vesicles, with a diameter of over 200 nm, while for pure poly(ODMACl−TANED), small rodlike particles with a mean diameter of the cross-section of 15.4 and a rod length of approximately 35−40 nm were observed.[23] Evidently, the incorporation of Brij 76 into poly(ODMACl−TANED) dramatically changes its morphology. When a molar ratio of Brij 76 to ODMACl is raised to 1:2, only a small amount of precipitate is formed upon TANED addition. The major part of the sample stays in the colloidal solution. The higher fraction of Brij 76 in the polymer particles (O-B76-T2-2, Brij 76/ODMACl = 1:2) causes the morphology change: the sample contains relatively irregular particles with a typical size of about 30 nm (Figure 1a, inset). When the sample is cast from methanol, the particles are larger (about 50 nm), but no vesicles were observed (not shown). It is noteworthy that, similar to poly(ODMACl−TANED), these polymer particles are formed because of the self-assembly of hydrophobic parts of polysilsesquioxane molecules consisting of ODMACl and TANED units with the inclusion of Brij molecules. Thus, reorganization of these polymer particles occurs easily depending on the solvent type and other conditions.

For Brij 78 at a molar ratio of Brij 78 to ODMACl of 1:6, the addition of TANED results in the formation of an opalescent colloidal solution: no precipitate is observed for months. Moreover, the reaction solution's stability depends on the equilibration time, that is, the time after ODMACl addition but before TANED addition: the stability increases 3-fold after 24 h (compared to 30 min or 2 h) of equilibration time. However, prolonged (24 h) equilibration also results in partial ODMACl condensation (revealed by line broadening in the ^{13}C NMR spectrum). Figure 1b shows the TEM image of the sample prepared from the O-B78-T2 reaction solution after ultrafiltration and stained with OsO_4. One can see fairly irregular particles with sizes in the 10−40 nm range. In the case of Brij 700, a similar morphology is observed, but the particles are larger, and the particle size distribution is even broader (image is not shown).

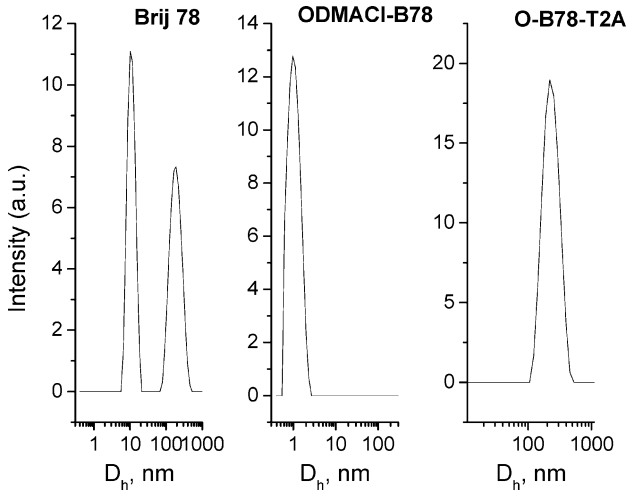

Figure 2. Hydrodynamic diameter distributions of Brij 78, the ODMACl−Brij 78 complex, and O-B78-T2 by dynamic light scattering.

To follow the formation of mixed particles, we used DLS measurements of the reaction solution based on Brij 78 after the incorporation of each reagent. Figure 2 shows hydrodynamic diameter distributions of the Brij 78 solution, the ODMACl−Brij78 complex, and O-B78-T2A obtained from DLS measurements. One can see that Brij 78 forms mainly micelles in aqueous solutions with a mean diameter of 11.3 nm and a small fraction of large aggregates with a mean diameter of 195 nm. Because the contribution of larger particles to the scattering intensity is much higher than that of the smaller particles (the scattering intensity is proportional to the squared volume, i.e., to R^6), the fraction of aggregates in the aqueous solution is negligible. The reaction solution examined 30 min after ODMACl addition shows nearly no micelles or micellar aggregates: the main species observed have a mean diameter of 1.1 nm, revealing a decomposition of Brij 78 micelles. The ODMACl solution of the same concentration contains mainly species with a mean diameter of about 1 nm and a small fraction of aggregates with a mean size of 52 nm, thus revealing that ODMACl alone also tends to form unimers or dimers instead of micelles in this solution. It is worth noting that the higher the concentration of ODMACl in an aqueous solution, the higher the fraction of methanol that is added (ODMACl is supplied as a 60% methanol solution), thus increasing the CMC of ODMACl in solution.

After 2 h of equilibration, similar observations were obtained except for a small fraction of micelles about 11 nm in diameter. After 24 h of equilibration, some fraction of large aggregates (∼150 nm) with a broad size distribution is formed along with 1.1 nm species. These findings suggest the following scenario depicted in Scheme 1. For simplicity of presentation, the molar ratio of Brij 78 to ODMACl is shown as 1:2. The addition of ODMACl results in the

Scheme 1. Schematic Representation of the Interaction of Brij, ODMACl, and TANED Molecules in an Aqueous Solution

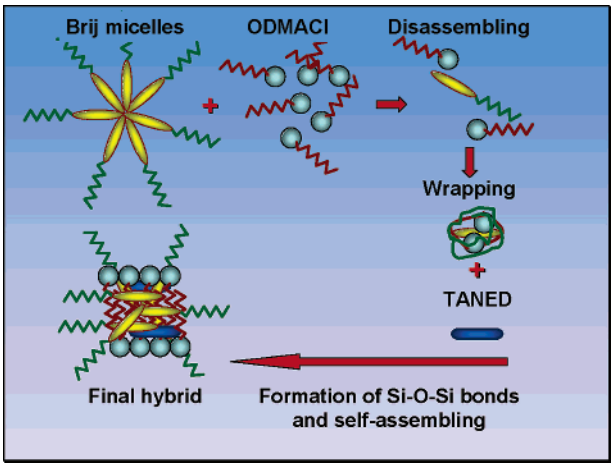

decomposition of Brij micelles because of binding of the hydrophobic tails of ODMACl to hydrophobic parts of Brij molecules as described elsewhere for SDS and Pluronics.[38−40] Unlike the interaction of PS-*b*-PEO block copolymer with anionic and cationic surfactants studied by us earlier,[31,32,46] here, no comicellization takes place. However, when TANED molecules are added, the formation of an electrolyte complex with ODMACl along with hydrolytic condensation and self-assembling lead to the formation of hybrid colloidal particles with a mean diameter of 244 nm (Figure 2). The apparent inconsistency in the size of the hybrid particles observed in TEM images and obtained from DLS measurements can be due to changes in the hybrid particles on the TEM grid initiated by an interaction with OsO_4 vapor. In the following sections, we will discuss the structure of these particles and verify the validity of this scheme.

1.2. Structure: ^{13}C NMR. To assess the fraction of the Brij molecules incorporated in the poly(ODMACl−TANED) structures, we used liquid-phase ^{13}C NMR in $CDCl_3$. Dissolution in chloroform destroys the hybrid structure formed by self-assembling hydrophobic tails, but the fraction of each component can be easily evaluated. Figure 3 (parts a and b) presents ^{13}C NMR spectra of the hybrid materials based on Brij 76 and Brij 78 and prepared at a molar ratio of 1:6. Both spectra show a signal at about 70 ppm assigned

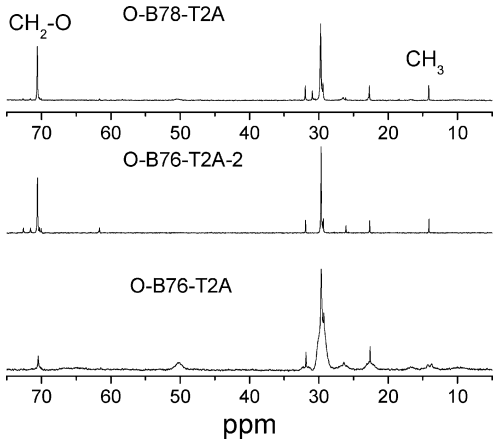

Figure 3. ^{13}C NMR spectra of O-B76-T2A, O-B76-T2A-2, and O-B78-T2A.

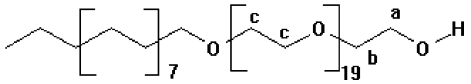

Figure 4. ^{13}C NMR spectrum of a mixture of Brij 78 and ODMACl. ODMACl resonances are marked with the pound sign; Brij 78 signals are marked with an asterisk, and signals used in the T_1 analysis are labeled a, b, and c, corresponding to the labels on the structure in Figure 5.

to central CH_2−O groups of Brij (see the Supporting Information for simulation spectra, Figures S1 and S2); however, the intensity of this signal is quite different. It is noteworthy that a number of signals observed in the ^{13}C NMR spectrum of ODMACl (Figure 4) practically disappear when the ODMACl−TANED gegenion is formed and condensation occurs (Figure 3) because of a pronounced line broadening for the carbon atoms of the methyl and methylene groups attached to N (10, 12, 13, and 14) and Si (1) (i.e., for all of the groups where mobility is impeded), as discussed in our preceding paper.[23]

To determine the relative amounts of the surfactants, we employed a ratio between the intensity of the Brij methylene signal at 70 ppm and the signal at 14 ppm assigned to terminal CH_3 groups of ODMACl and Brij using the formula $I_{CH2-O}/(I_{CH3}A) = x/(x + 1)$, where A is the number of the methylene groups included in the signal at 70 ppm (13 for Brij 76 and 33 for Brij 78) and x is the mole fraction of Brij to ODMACl.

Although both kinds of hybrid particles were prepared at the same molar ratio, for O-B76-T2A, the Brij to ODMACl molar ratio is 1:24, while for O-B78-T2A, this value is 1:4.3. We think that, when TANED is added, the shorter surfactant does not provide stability to the complex, so condensation of the ODMACl−TANED mixture leads to precipitation and the expulsion of the majority of Brij 76 molecules from the condensate. For longer PEG chains, the hybrid micellar structures form after the addition of TANED, so no precipitation takes place, although the degree of condensation is the same (see discussion below). It is worth noting that the Brij 78 fraction in O-B78-T2A is slightly higher than the one from the loading (0.23 vs 0.17), possibly reflecting a preferred structure for the complex between Brij 78 and ODMACl. When the fraction of Brij 76 molecules is increased by a factor of 3 (O-B76-T2A-2), the incorporation of Brij molecules is nearly complete, reaching a molar ratio of 1:1.8 for Brij 76 to ODMACl (mol). As discussed above, most of the product remains suspended as colloids. Comparison of the ^{13}C and ^{29}Si NMR spectra of samples isolated from the precipitate and from the colloidal solution of O-B76-T2A-2 and dissolved in deuterated chloroform shows that they are fully identical, indicating that the partial precipitation is caused by limited solubility. The hybrid particles with Brij 700 are only marginally soluble in chloroform (because of high PEG crystallinity), so a ^{13}C NMR spectrum was acquired in the solid state. This spectrum shows a much lower fraction of PEG units than that in O-B78-T2A, indicating that there are steric hindrances in the formation of hybrid micellar structures with this surfactant. However, a direct quantitative comparison with the liquid-phase NMR data is not possible.

1.3. Relaxation: ^{13}C NMR. To confirm that ODMACl molecules do disintegrate Brij micelles and bind to them,

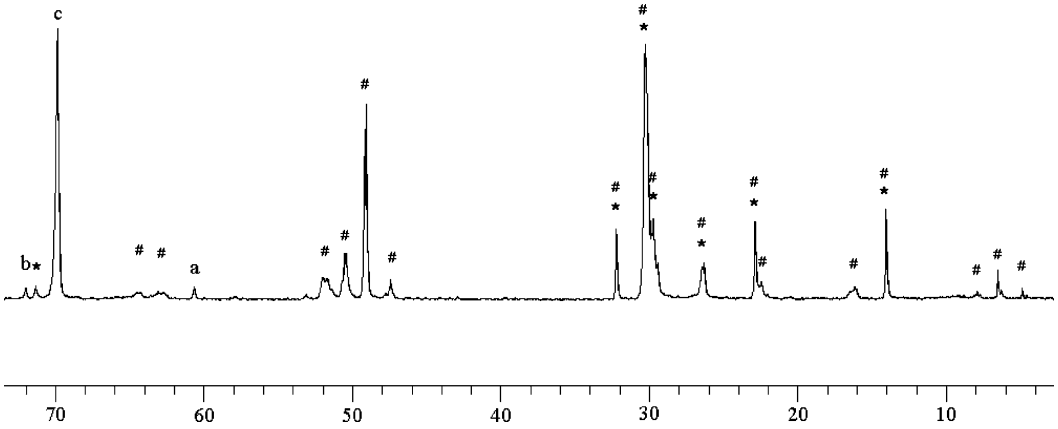

Figure 5. Brij 78. Carbons whose signals were resolved from ODMACl are labeled a, b, and c.

we did a qualitative study of NMR relaxation. ^{13}C T_1 measurements were determined for Brij 78, ODMACl, and Brij 78−ODMACl hybrid solutions in D_2O at 25 °C. To ensure easier acquisition of the NMR data, we used a 6-fold concentration of both reagents compared to those used in the procedure described in the Experimental section. It is noteworthy that the DLS data for the Brij 78, ODMACl, and Brij 78−ODMACl complex solutions used for relaxation measurements (6-fold concentration) practically coincide with those obtained for reaction solutions, thus making the comparison of DLS and relaxation NMR data plausible.

Only three resonances could reliably be compared between the two sets of spectra (Brij 78 and ODMACl−Brij 78) because all others either overlapped with signals from the ODMACl or were too weak for an accurate T_1 determination. The signals used are annotated on the spectrum in Figure 4, and their corresponding carbons are labeled in Figure 5.

The signals for which T_1 values were compared were the central polyethoxy methylenes (c) and the two methylene groups at the terminal hydroxyl (a and b). In each case, the T_1 values were higher in the complex than in the Brij 78 micelles, which is consistent with the increased effective correlation time one would expect with the breakup of the Brij micelle when the mobility of these carbons is higher. This is, of course, assuming that the correlation times of the Brij PEG chain carbons are on the order of 10^{-10} s or less, which would be expected because such correlation times have been reported previously for very large PEO systems.[47] The greatest increase (51 ± 10%) was observed with the methylene group at the terminal hydroxyl (a), and the smallest effect (13%, a change smaller than the standard error of 15%) was at the neighboring methylene (b). Central polyethoxy methylenes (c) experienced an overall T_1 increase of 17 ± 0.5%; however, individual contributions could not be assessed. We think that PEG tails in the unimer complexes are unrestricted and may easily fold, wrapping around the hydrophobic core formed by $C_{18}H_{37}$ tails of both ODMACl and Brij 78 (Scheme 1). The ability of PEO chains to wrap around a hydrophobic core was reported in ref 48.

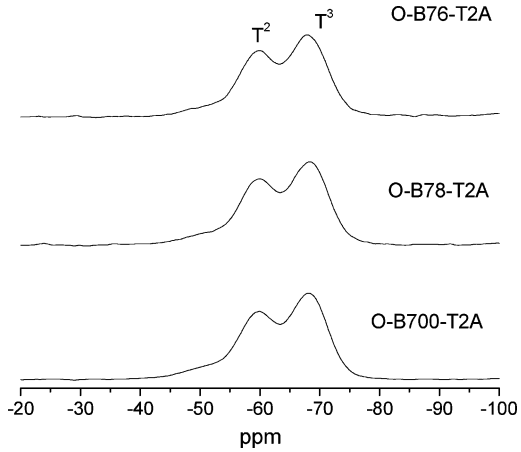

Figure 6. Solid-state CP/MAS ^{29}Si NMR spectra of O-B76-T2A, O-B78-T2A, and O-B700-T2A.

Additional evidence of hydrophobic interactions in the Brij 78−ODMACl mixture comes from the noticeable line broadening (from half-height line widths) of the ^1H NMR signals (see the Supporting Information, Figure S3), belonging to methylenes of the hydrophobic regions of ODMACl, especially of those adjacent to the quaternary ammonium group, reflecting the lower mobility of these groups. In addition, the peak containing the Brij PEG methylenes reveals just the opposite, a sharpening of the signal upon combining with ODMACl. Again, this is what one might expect as the Brij molecules go from a slow-moving micelle to a faster-moving unimer complex with ODMACl. Thus, the NMR data corroborate the conclusion derived from DLS on the decomposition of Brij micelles in the presence of ODMACl and the formation of the ODMACl−Brij 78 complex.

2. Structure and Mobility in the Solid State. *2.1. Structure: ^{29}Si NMR and FT-IR.* Poly(ODMACl−TANED) macromolecules are well-soluble in chloroform, so liquid-phase ^{29}Si NMR was employed.[23] However, the comparatively poor solubility (due to PEG crystallinity) of the hybrid particles in chloroform makes it unfeasible to acquire the ^{29}Si NMR spectra in the liquid phase, so solid-state ^{29}Si CP/MAS NMR has been used. The ^{29}Si NMR spectra of O-B76-T2A, O-B78-T2A, and O-B700-T2A (Figure 6) indicate that two types of Si species are present in these materials: T^2 [R−Si(OH)O_2] and T^3 [R−Si$O_{3/2}$], and the latter prevails.

(47) Chari, K.; Antalek, B.; Lin, M. Y.; Sinha, S. K. *J. Chem. Phys.* **1994**, *100*, 5294.
(48) Lo Celso, F.; Triolo, A.; Bronstein, L.; Zwanziger, J.; Strunz, P.; Lin, J. S.; Crapanzano, L.; Triolo, R. *Appl. Phys. A.* **2002**, *74*, S540.

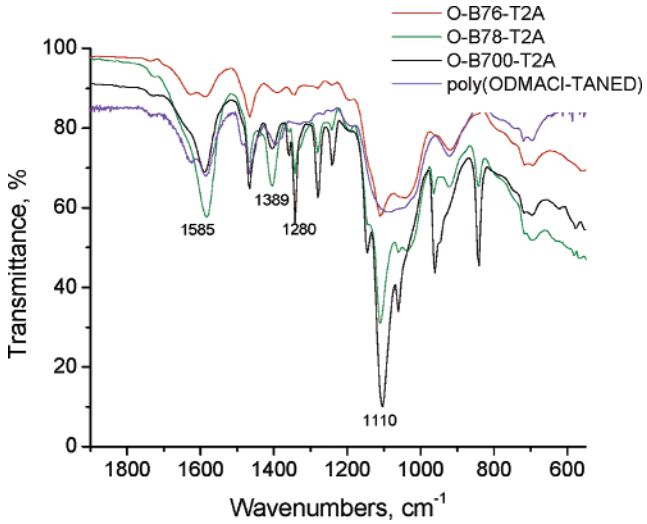

Figure 7. FT-IR spectra of O-B76-T2A, O-B78-T2A, O-B700-T2A, and poly(ODMACl−TANED).

This demonstrates a considerably high degree of condensation [higher than that of pure poly(ODMACl−TANED)[23]], revealing that the presence of surfactant molecules does not thwart the hydrolytic condensation but, conversely, facilitates it. One can see that the degree of condensation does not depend on the surfactant structure (Figure 6), fraction, or equilibration time (not shown). On the other hand, as discussed above, the degree of surfactant incorporation is very sensitive to the given parameters.

Figure 7 presents the FT-IR spectra of hybrid polymer particles. Similar to that of poly(ODMACl−TANED), these spectra contain bands at 1585 and 1389 cm^{-1}, characteristic of the carboxylate ion.[49] This unambiguously confirms the incorporation of TANED molecules in the Brij-modified hybrid polymer colloids. In addition, the spectra contain bands at 1280 and 1110 cm^{-1} assigned to CH_2 deformation and C−O−C stretching, respectively, typical for PEG units.[50] The intensity of these bands is consistent with the fraction of PEO tails obtained from the ^{13}C NMR data.

2.2. Structure: DSC and XRD. In these studies, we primarily focused on two surfactants: Brij 76 and Brij 78. Their DSC traces were compared with those of hybrid materials (Figure 8). The DSC trace of Brij 76 shows a glass transition with a fictive temperature of −65 °C, a strong endothermic peak at 36 °C with ΔH = 50.5 J/g, and two very weak, broad transitions at −18 and +17 °C. Conversely, the DSC trace of Brij 78 shows no glass transition, but it does show the major endothermic peak at 45 °C with ΔH = 99.0 J/g. Both Brij surfactants studied here contain a $C_{18}H_{37}$ (octadecyl) hydrophobic tail and a PEG tail of a different length: 440 Da for the PEG in Brij 76 and 880 Da for the PEG in Brij 78. Normally, PEGs of a molecular weight of about 500−600 Da are fully amorphous at room temperature.[51] Then, for Brij 76, the endothermic peak at 36 °C might be assigned to the melting of a crystalline phase because of octadecyl tail ordering. Weak broad peaks at −18 and +17 °C may be due to a disordered interphase including both octadecyl and PEG fragments and a PEG phase,[51] respectively. Because no glass transition is observed for Brij 78, one can assume that Brij 78 PEG is either nearly fully crystalline or the amorphous regions are well-spread between the crystalline regions, restricting PEG chain mobility and thus suppressing the glass transition. An endothermic peak at 45 °C is due to both PEG and octadecyl tail structure melting. Although the DSC traces of Brij 76 and 78 are so different, a comparison of their XRD profiles (Table 2) shows significant similarities: both show two sharp peaks at s values of 13.9 and 16.5 nm^{-1} (Figure 9), representing the crystalline peaks of the PEO domain,[52] although for Brij 76, these peaks are much weaker. On the other hand, the width and intensity of the signal at 16.5 nm^{-1} for both samples reveals the contribution of the other crystalline phase, attributed to octadecyl tails. Thus, despite low molecular weights of PEG blocks with 10 and 20 repeated units, they are both at least semicrystalline, and both Brij surfactants are polymorphic.

Table 2. Structural Parameters from XRD

sample	s, nm	d, nm
Brij76	13.9	0.45
	15.4	0.41
	16.5	0.38
	18.9	0.33
	25.6	0.25
Brij78	13.8	0.46
	16.6	0.38
	18.9	0.33
	25.2	0.25
O-B76-T2	15.3	0.41
O-B78-T2	13.8	0.45
	15.9	0.39
	16.7	0.38
poly(O-T)	14.4	0.44

The hybrid material containing Brij 76 (O-B76-T2A) displays a glass transition with a T_g of −38 °C and two endothermic peaks, the smaller one at 37 °C (ΔH = 0.8 J/g) and the larger one at 55 °C (ΔH = 16.8 J/g). We believe that the increase in the glass transition temperature of PEG tails from −65 °C for Brij 76 to −38 °C for O-B76-T2A is due to immobilization of the octadecyl tail within the poly(ODMACl−TANED) polysilsesquioxane structure, decreasing PEG tail mobility. A weak endothermic transition at 37 °C can be assigned to the melting of the PEG crystalline phase of the surfactant, while a strong transition at 55 °C should be responsible for a crystalline phase formed by $C_{18}H_{37}$ tails from both ODMACl and Brij 76 molecules. It is worth noting that poly(ODMACl−TANED) does not display any transitions in the temperature range studied, while pure poly(ODMACl) (PODMACl) shows an endothermic peak in the range 40−60 °C due to melting of the PODMACl crystalline phase.[23] At the same time, the X-ray diffraction pattern of O-B76-T2A (Figure 10a) shows a pronounced amorphous halo similar to that of poly(ODMACl−TANED),[23] the position of which is similar to that of PODMACl.[23] Applying Bragg's Law,[53] $d = \lambda/(2 \sin \theta)$, with λ = 1.5418

(49) Tajmir-Riahi, H. A. *J. Inorg. Biochem.* **1990**, *39*, 33.
(50) Chen, H.; Jiang, C.; Wu, H.; Chang, F. *J. Appl. Polym. Sci.* **2004**, *91*, 1207.
(51) Salamone, J. C. *Polymeric Materials Encyclopedia*; CRC Press: Boca Raton, FL, 1996; Vol. 8.
(52) Yeh, S.-W.; Wu, T.-L.; Wei, K.-H.; Sun, Y.-S.; Liang, K. S. *J. Polym. Sci. Phys.* **2005**, *43*, 1220.
(53) Klug, H. P.; Alexander, L. E. *X-ray Diffraction Procedures for Polycrystalline and Amorphous Materials*; Wiley: New York, 1970.

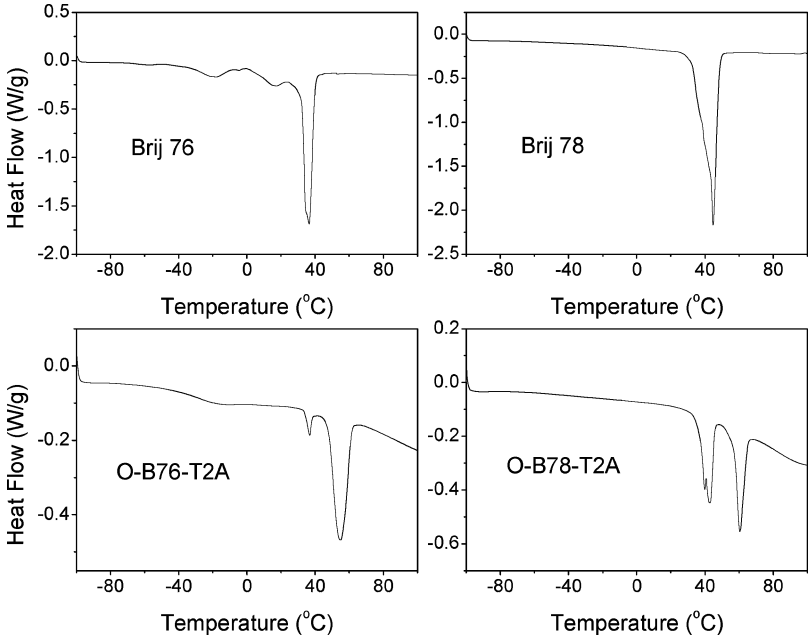

Figure 8. DSC traces of Brij 76, Brij 78, O-B76-T2A, and O-B78-T2A.

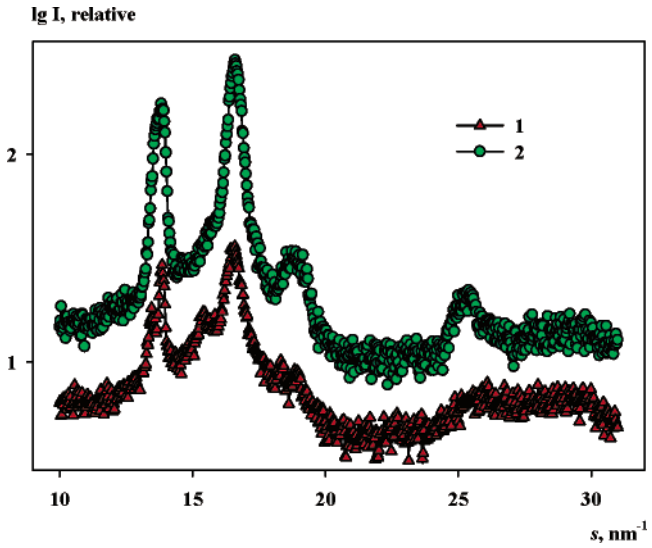

Figure 9. XRD profiles of Brij 76 (1) and Brij 78 (2).

Å and a peak position $s = 15.4$ nm^{-1}, one obtains a d spacing of 4.13 Å. This value is close to the chain−chain spacing observed in dense phases of alkyl chains.[54] The weak reflections at $s = 13.9$ and 16.5 nm^{-1} typical for the PEO crystalline phase might be concealed under the broad amorphous peak, so no conclusion on the PEO crystallinity in this sample can be made.

The DSC profile of the O-B78-T2A hybrid (Figure 8) displays two endothermic peaks at 43 ($\Delta H = 13.40$ J/g) and 60 °C ($\Delta H = 11.82$ J/g), the former peak containing a shoulder at 42 °C. This complex trace is consistent with the polymorphism reflected by the XRD profile of this sample (Figure 10b): it contains two broad peaks at 13.9 and 16.5 nm^{-1} (Table 2), which can be assigned to the PEO crystalline phase, and a broad reflection at 15.4 nm^{-1} typical for dense packing of the alkyl chains (as in O-B76-T2A). Thus, similar to Brij 78, O-B78-T2A is at least semicrystalline and polymorphic.

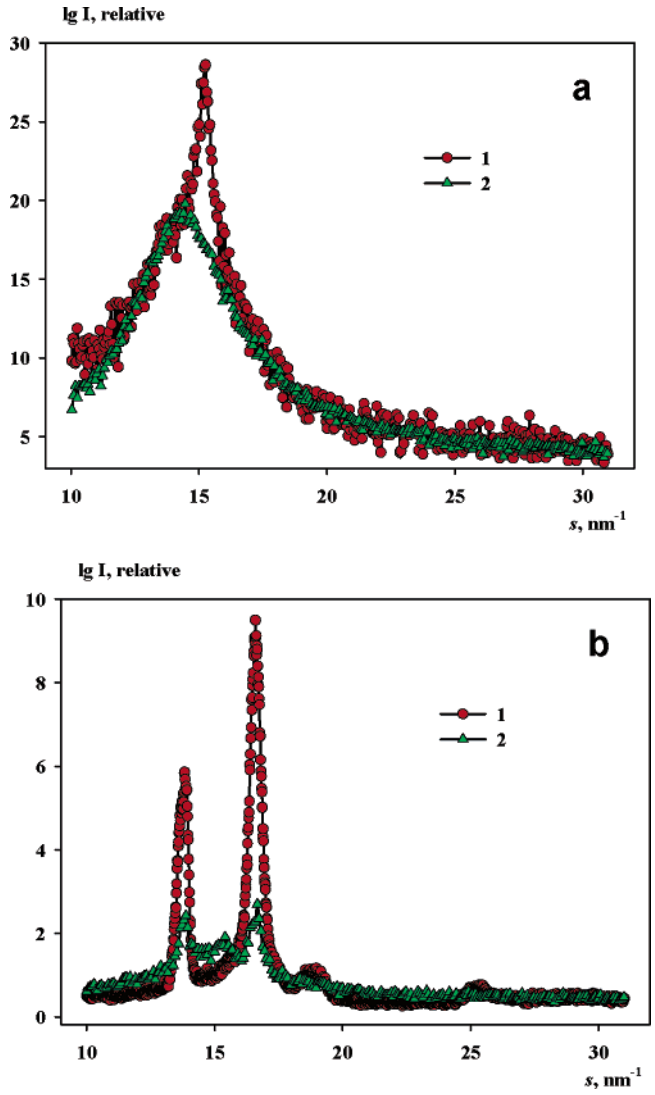

Figure 10. XRD profiles of (a) O-B76-T2A (1) and poly(ODMACl−TANED) (2) and (b) Brij 78 (1) and O-B78-T2A (2).

(54) Parikh, A. N.; Schivley, M. A.; Koo, E.; Seshadri, K.; Aurentz, D.; Mueller, K.; Allara, D. L. *J. Am. Chem. Soc.* **1997**, *119*, 3135.

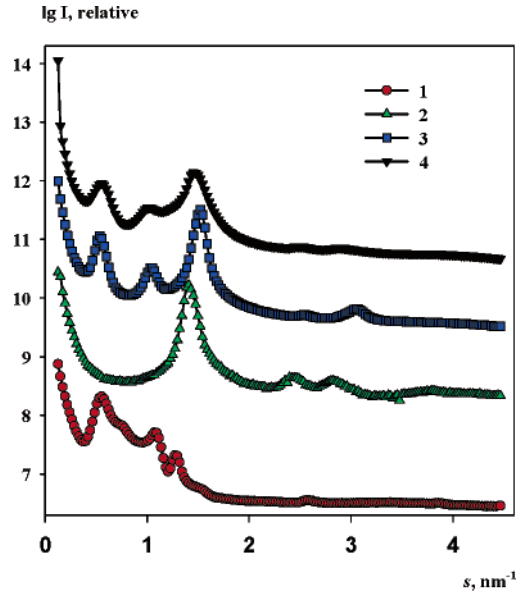

Figure 11. SAXS profiles of Brij 76 (1), O-B76-T2A (2), O-B76-T2-2A-prec (precipitate) (3), and O-B76-T2A-2-sol (the solid obtained by evaporation of the colloidal solution) (4).

2.3. Structure: SAXS. To evaluate the organization of the hybrid materials in the solid state, a SAXS study was performed. Self-assembling systems are known to adopt a wide variety of structures on the nanoscopic scale. Basic structures formed at a low concentration of surfactants are spherical micelles, cylinders, and plane surfaces, while at higher concentrations, micelles on the cubic lattice, cylinders on the 2D hexagonal lattice, and plane membranes on lamellar phases can be observed.[55−59] The sample morphology generally depends on the type and ratio of hydrophilic and hydrophobic moieties, but the crystallization of a surfactant hydrophilic block (such as PEG in our case) can completely alter the morphology.[60] Table 3 summarizes the calculated structural characteristics from the present SAXS investigation, corresponding to the entire spectrum of ordered structures in the Brij-based hybrid materials.

The pure surfactant molecules of Brij 76 (Figure 11, curve 1) self-assemble, forming a cubic phase with a lattice size $d_c = 11.5$ nm and a moderate degree of disorder $\Delta/d_1 = 0.10$ (Table 3). It is reasonable to assume that the cubic phase is built from the densely packed Brij 76 micelles. If the latter were formed by a fully extended $C_{18}H_{37}$ (1.7 nm) and 10-unit PEG (3.1 nm) tails, their diameter would be about 9.6 nm (Scheme 2). It should be noted that, because PEG-chain self-assembly occurs during the evaporation of aqueous solutions at 60 °C (above the melting point of all of the components), the PEG tails may not adopt the extended conformation.[61] The observed periodicity of the cubic phase is therefore somewhat larger than expected, which can be explained by the retention of water in hydrophilic regions as indicated in ref 57.

Scheme 2. Schematic Representation of Brij 76−ODMACl−TANED Bilayer (bottom)[a]

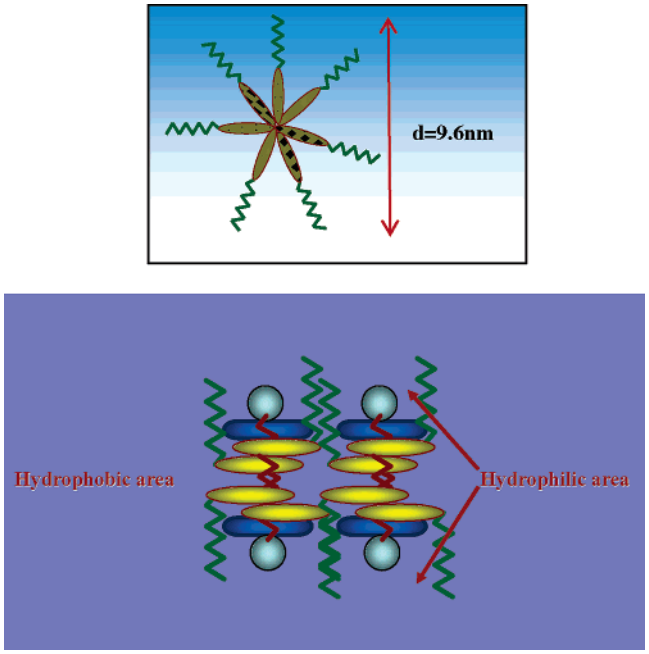

[a] The same color coding as in Scheme 1 has been used.

The structure of the Brij 76 based hybrid material depends on the Brij to ODMACl molar ratio. At the loading ratio of 1:6 (curve 2, O-B76-T2A), resulting in an actual ratio of 1:24 (see section 1.2), a two-dimensional hexagonal packing with a distance between the micelles of $d_{hex} = 5.1$ nm takes place. The same packing has been already observed for the poly(ODMACl−TANED) samples,[23] which indicates that, at this low content, Brij 76 does not significantly alter the structure of the binary composite.

When the loading of Brij 76 is increased by a factor of 3 (O-B76-T2A-2), resulting in an actual Brij to ODMACl molar ratio of 1:1.8 (see section 1.2), no immediate precipitation occurs upon TANED addition. After about 30 min, some amount of precipitate forms (curve 3), but most of the polymer stays in the colloidal solution (curve 4, after water evaporation). The two materials are chemically identical (see section 1.2) but exhibit different organizations. The precipitate forms a lamellar structure with the repeat of $d_l = 11.6$ nm nearly coinciding with that of the cubic Brij 76 phase, which suggests that the lamellae are mainly formed by the Brij 76 bilayers. A possible model of the hybrid lamellar structure is presented in Scheme 2 (bottom), where the poly(ODMACl−TANED) composites are located in the central, largely hydrophobic part of the bilayer. The soluble material is less ordered, and its structure can be described as a texture[45] with a larger major periodicity of 16.0 nm. In this case, poly(ODMACl−TANED) composites may again enter into the central part of Brij 76 micelles, but the hybrid assemblies have a preferential orientation (poorly ordered cylindrical shapes with quasi-2D packing), leading to the arrangement illustrated in Scheme 3.

As one can see from Figure 12 (curve 1) and Table 3, Brij 78 forms a well-ordered lamellar structure with a

(55) Li, X.; Kunieda, H. *Langmuir* **2000**, *16*, 10092.
(56) Merta, J.; Torkkeli, M.; Ikonen, T.; Serimaa, R.; Stenius, P. *Macromolecules* **2001**, *34*, 2937.
(57) Garstecki, P.; Holyst, R. *Langmuir* **2002**, *18*, 2519.
(58) Garstecki, P.; Holyst, R. *Langmuir* **2002**, *18*, 2529.
(59) Rappolt, M.; Hickel, A.; Bringezu, F.; Lohner, K. *Biophys. J.* **2003**, *84*, 3111.
(60) Hillmyer, M. A.; Bates, F. S. *Macromol. Symp.* **1997**, *117*, 121.
(61) Smarsly, B.; Polarz, S.; Antonietti, M. *J. Phys. Chem. B* **2001**, *105*, 10473.

Table 3. Structural Characteristics of the Brij-based Hybrid Materials

composition	s, nm^{-1}	L, nm	$\Delta/\bar{d}$	ratio s_n/s_1	Miller indices	type of packing and distance between micelles, nm
Brij 76	0.55	128.9	0.10	1	100	cubic $d_c = 11.5$
	0.76			1.38	110	
	1.09			1.98	200	
	1.28			2.33	210	
	1.44			2.62	211	
	2.01			3.65	320	
	2.58			4.69	421	
	3.87			7.04	550	
Brij 78	0.40	160.5	0.08	1	100	lamellar $d_l = 15.7$
	0.79			1.98	200	
	1.18			2.95	300	
	1.57			3.92	400	
	2.74			6.9	500	
	3.15			7.9	600	
	3.54			8.9	700	
	3.94			9.8	800	
Brij 700	0.29	163.7	0.09		110	cubic $d_c = 30.6$
	0.47			1.62	210	
	0.93			3.21	420	
	1.10			3.79	432	
	1.43			4.93	444	
	1.91			6.58	664	
	2.21			7.62	864	
	2.68			9.24	886	
O-B76-T2A (1:6; 30 min)	1.42	54.6	0.09	1	10	2D hexagonal $d_{hex} = 5.1$
	2.43			1.7	11	
	2.84			2.0	20	
	3.73			2.6	21	
O-B76-T2A-prec (1:2; 30 min)	0.54	106.7	0.10	1	100	lamellar $d_l = 11.6$
	1.04			2.0	200	
	1.52			3.0	300	
	2.55			5.1	400	
	3.05			6.0	500	
O-B76-T2A-sol (1:2; 30 min)	0.56	86.8	0.11	1	011	texture $d = 16.0$
	1.00			1.78	112	
	1.39			2.48	222	
	1.86			3.32	332	
	2.51			4.48	442	
	2.90			5.17	552	
O-B78-T2A (1:6; 30 min)	0.42	181.7	0.09	1		cubic $d_c = 11.0$ (coexisting with lamellar $d_l = 11.6$)
	0.76			1.81		
	1.46			3.48		
	1.62			3.86		
	2.54			6.04		
	2.92			6.95		
	3.40			8.09		
O-B78-T2 (1:6; 2 h)	0.74	132.8	0.08	1	110	cubic $d_c = 12.0$
	1.70			2.29	311	
	3.41			4.61	621	
O-B78-T2B (1:6; 24 h)	0.72	99.9	0.09	1	110	cubic $d_c = 12.4$
	1.53			2.12	220	
	2.65			3.68	333	
	3.05			4.24	442	
	4.05			5.63	651	
O-B700-T2A (1:6; 30 min)	0.53	106.6	0.11	1	110	cubic $d_c = 16.8$
	1.12			2.11	221	
	1.25			2.36	311	
	1.61			3.04	411	
	2.72			5.13	551	
O-B78-T2B-Fe_2O_3 (1:6; 24 h)	1.5	48.01	0.09	1	100	lamellar d_l =4.2
	3.1			2	200	

periodicity of 15.7 nm. This size neatly matches the extended conformation of a double Brij 78 layer (~15.4 nm), indicating a normal lamellar packing of the bilayers. In contrast to other oligo(oxyethylene) mono-*n*-alkyl ethers,[62] no tilting of the hydrophobic tails is observed in Brij 78 lamellae. The peaks in the scattering pattern from the hybrid material O-B78-T2A after a 30 min equilibration (Figure 12, curve 2) can be interpreted differently. On one hand, they can be attributed to a cubic phase with a periodicity of 21.4 nm (Table 3). On the other hand, the first maxima are at nearly the same positions as those in Brij 78 alone, although these peaks appear somewhat smeared. This latter observation may indicate that a fraction of less-ordered Brij 78 lamella coexist with the cubic phase formed in the hybrid material. This emerging cubic phase with a period of about 12 nm manifests itself more clearly after a 2 h equilibration time (O-B78-T2,

(62) Craven, J. R.; Hao, Z.; Booth, C. *J. Chem. Soc., Faraday Trans.* **1991**, *87*, 1183.

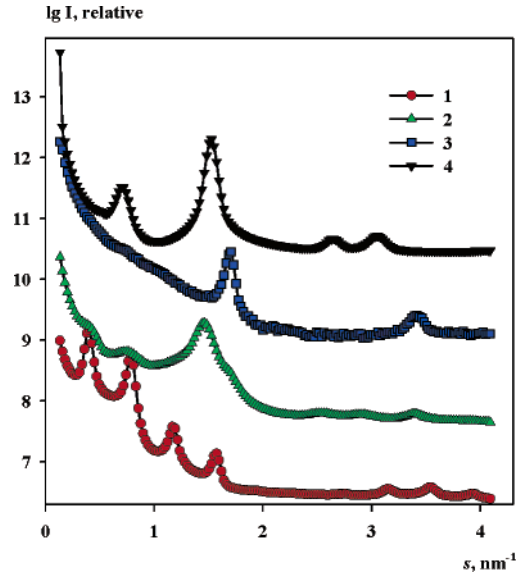

Figure 12. SAXS profiles of Brij 78 (1), O-B78-T2A (2), O-B78-T2 (3), and O-B78-T2B (4).

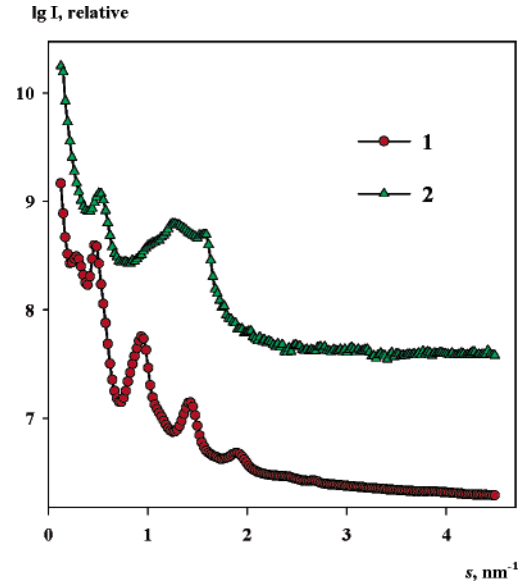

Figure 13. SAXS profiles of Brij 700 (1) and O-B700-T2A (2).

Scheme 3. Schematic Illustration of Brij 76 Based Composite Texture

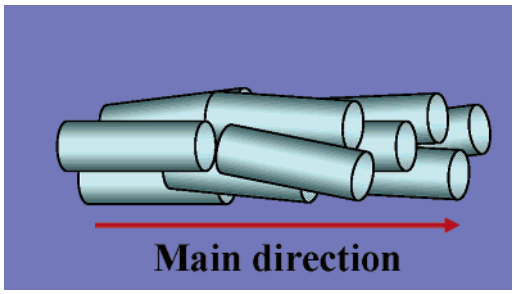

Scheme 4. Schematic Illustration of Multiply Folded Tails of Brij 700 Surfactant

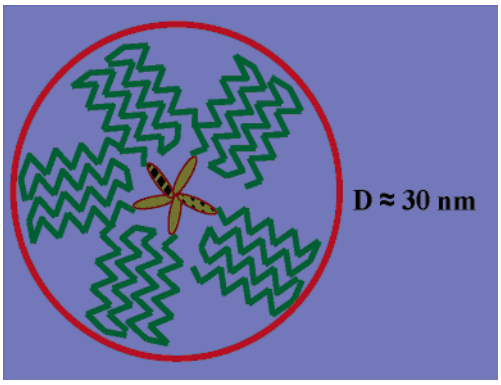

curve 3) although the maxima are still not pronounced. Prolongation of the equilibration time up to 24 h (O-B78-T2B) shows a set of distinct maxima corresponding to the cubic phase, whereas the lamellar phase disappears completely.

The scattering patterns of Brij 700 and the Brij 700 based hybrid material are presented in Figure 13. The surfactant alone reveals a cubic phase with a lattice constant of 30.6 nm. Given that the width of the fully extended Brij 700 bilayer is about 75 nm, this result is compatible with a folded-back configuration of the hydrophilic tails in the micelles packed into the cubic phase. The hybrid material O-B700-T2A reveals a texture-like structure similar to that of O-B76-T2A-sol with nearly the same period (16.8 nm). This suggests that the PEG tails of O-B700-T2A are multiply folded (Scheme 4) to yield the same diameter of the cylindrical hybrid micelles in the texture.

Overall, the SAXS data indicate that the structure of the hybrid solids significantly depends on the surfactant structure and on its mole fraction in the hybrid particles, and very different types of packing were observed. The 2D hexagonal phase and texture are formed by "closed" particles, represented by cylindrical micelles in the case of hexagonal organization, and rodlike micelles for the texture. The lamellae form a continuous medium not consisting of separate particles. Closed micelles can be formed from the continuous phase because of a line defect or partial disordering of the lamellar layers.[59] Interestingly, the type of ordering in hybrid systems does not seem to be related to the initial ordering of the surfactant. Indeed, pure Brij 76 forms a cubic phase, but the hybrid materials were 2D hexagonal, lamella, and texture phases; the lamellar packing in Brij 78 alone was replaced by cubic phases in the hybrid materials (Table 3). It is also worth noting that the degree of disorder in all systems including pure surfactants is in the range 0.09−0.11, typical for a polymer system with crystalline regions coexisting with disordered bicontinuous phases.

3. Templating with Hybrid Particles. To illustrate the possibility of using the hybrid particles as soluble templates for nanoparticle formation, we studied the formation of iron oxide nanoparticles within these hybrid polymer colloids. The latter were first loaded with Fe(II) ions at a molar ratio of COONa to $(NH_4)_2Fe(SO_4)_2$ of 3:1, followed by oxidation with hydrogen peroxide at pH 10. It should be noted that, because TANED carboxylic groups form gegenions with quaternary ammonium groups of ODMACl, the incorporation of Fe(II) ions requires extended time (at least 2−3 days) to replace quaternary ammonium cations with Fe(II) ions. To facilitate the incorporation of Fe(II) ions, NaCl can be added to the solution of the hybrid particles (1 M NaCl), allowing one to accomplish reaction for 8−10 h. Further oxidation of this sample should result in the formation of iron oxide

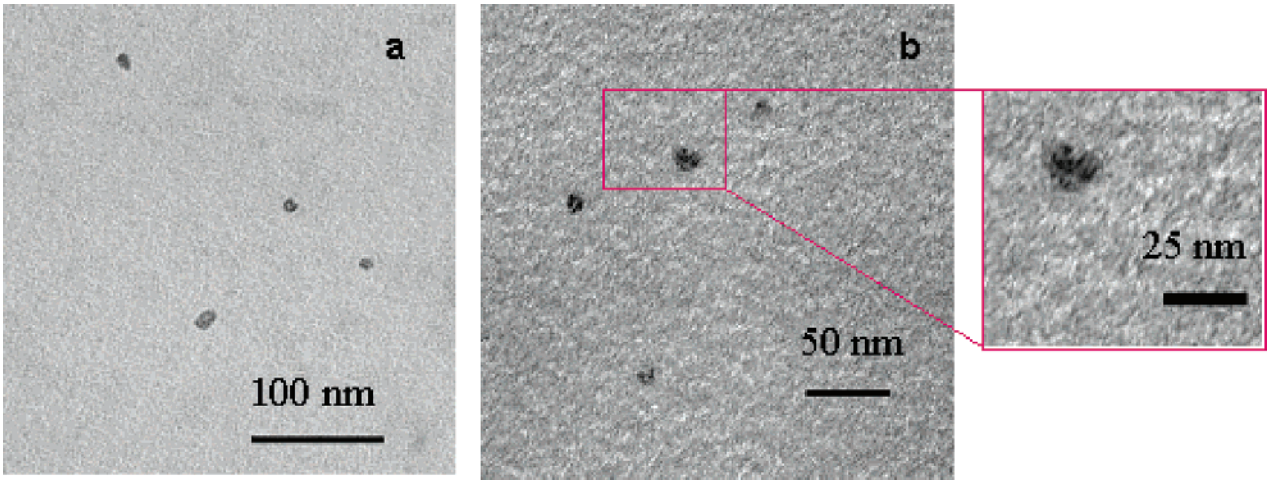

Figure 14. TEM images of (a) O-B78-T2B-Fe(II) and (b) O-B78-T2B-Fe_2O_3.

nanoparticles.[11] By elemental analysis, the iron content in O-B78-T2B-Fe_2O_3 is 5.30 wt %; ~78% of the calculated amount according to the iron salt loading.

Figure 14a shows the TEM image of the O-B78-T2B-Fe(II) particles after the incorporation of iron ions. The presence of Fe species provides a needed contrast, so no staining is required for colloidal particle visualization. This eliminates a possibility of alteration of the polymer particle structure on the TEM grid under staining conditions (see discussion above). Because the hybrid particles are formed as a result of the self-assembly of hydrophobic tails, they are easily rearranged. Variation of the environment or particle composition [here, the presence of Fe(II) ions] leads to changes of the particle characteristics. The O-B78-T2B-Fe(II) particles measure 8.7 nm in diameter and have a narrower size distribution than parent O-B78-T2B particles. The mean particle diameter after oxidation (Figure 14b) is 9 nm, revealing nearly no change in hybrid particle characteristics. The available resolution of the TEM instrument does not allow us to accurately measure the Fe_2O_3 nanoparticles' size, although a rough estimation gives sizes in the range of 1−1.5 nm. The XRD profile shows no reflections typical for an iron oxide crystalline phase; this can be attributed both to the small size and to the amorphous character of iron oxide particles prepared in ambient conditions. Overall, Figure 14 demonstrates that neither the incorporation of guest ions such as Fe(II) nor that of guest particles such as iron oxide leads to the aggregation of polymer colloids because of the protective PEG shell.

The guest particles in these systems are much smaller than the iron oxide nanoparticles formed in the pores of polysiloxane frameworks containing amino groups[63] or in the hybrid network diurasils.[64] We think that, unlike mentioned literature precedents, the presence of hydrophobic tail ordering in our systems additionally controls nanoparticle formation.

Figure 15 demonstrates that the structure of the hybrid material changes upon the formation of Fe_2O_3 nanoparticles.

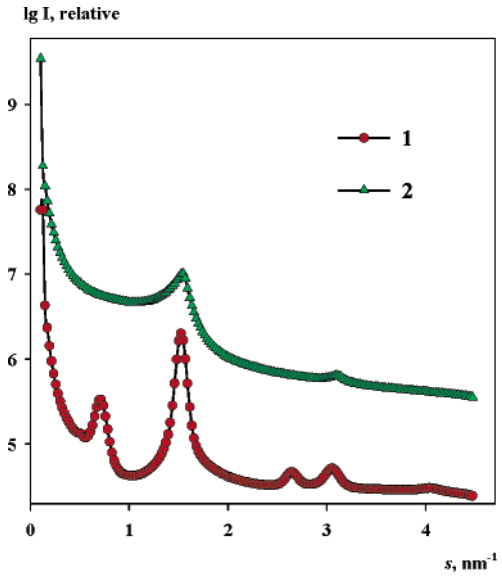

Figure 15. SAXS profiles of O-B78-T2B (1) and O-B78-T2B-Fe_2O_3 (2).

Instead of the cubic phase in O-B78-T2B (see the discussion of Figure 12), a poorly ordered lamellar phase with a period of $d_l = 4.2$ nm is formed. This significant alteration of the internal structure is observed despite the small Fe_2O_3 nanoparticle sizes, which should not have disturbed the packing. We attribute this phenomenon to an increase in the hydrophilicity of the system after the incorporation of Fe(II) ions and nanoparticle formation.

Conclusion

We synthesized and characterized hybrid polymer particles with a protective PEG shell on the basis of hydrolytic condensation and the self-assembly of two silanes, ODMACl and TANED, and Brij surfactants. The interaction between Brij and ODMACl was followed with NMR and DLS, while hybrid structures formed after the addition of TANED were studied using TEM, NMR, and DLS. These methods revealed that the addition of ODMACl leads to the disintegration of Brij micelles and the formation of unimer Brij−ODMACl complexes. The interaction of these complexes with TANED in aqueous solutions results in the formation of large hybrid particles with a mean diameter of 244 nm. The incorporation

(63) Rao, M. S.; Dubenko, I. S.; Roy, S.; Ali, N.; Dave, B. C. *J. Am. Chem. Soc.* **2001**, *123*, 1511.
(64) Silva, N. J. O.; Amaral, V. S.; de Zea Bermudez, V.; Nunes, S. C.; Ostrovskii, D.; Rocha, J.; Carlos, L. D. *J. Mater. Chem.* **2005**, *15*, 484.

of guest ions such as Fe(II) or the formation of nanoparticles therein does not result in the aggregation of hybrid polymer colloids because of the PEG protective shell afforded by Brij surfactants.

The evaporation of purified reaction solutions at 60 °C (above the melting transitions of all of the components) leads to various structures and morphologies, the type and characteristics of which depend on the hybrid particle composition. The internal structure of the solid surfactants and hybrid structures was comprehensively characterized by SAXS. For the shortest surfactant, Brij 76, a lamellar morphology of the hybrid sample is obtained when the Brij to ODMACl molar ratio is close to 1:2. For hybrid materials based on Brij 78 or Brij 700, cubic structures are usually observed. When iron oxide nanoparticles are formed in the hybrid particles, poorly ordered lamellae are formed instead of cubic structures.

Acknowledgment. This work has been supported, in part, by the NATO Science for Peace Program (Grant SfP-974173) and, in part, by NSF Grant BES-0322767. The authors thank Dr. Maren Pink for X-ray diffraction measurements.

Supporting Information Available: NMR simulation spectra and ^{1}H NMR spectra. This material is available free of charge via the Internet at http://pubs.acs.org.

CM060129T